Improved Performance of Bayesian Solutions for Inverse Electrocardiography Using Multiple Information Sources

Yeşim Serinagaoglu*, *Member, IEEE*, Dana H. Brooks, *Senior Member, IEEE*, and Robert S. MacLeod, *Member, IEEE*

***Abstract*—The usual goal in inverse electrocardiography (ECG) is to reconstruct cardiac electrical sources from body surface potentials and a mathematical model that relates the sources to the measurements. Due to attenuation and smoothing that occurs in the thorax, the inverse ECG problem is ill-posed and imposition of *a priori* constraints is needed to combat this ill-posedness. When the problem is posed in terms of reconstructing heart surface potentials, solutions have not yet achieved clinical utility; limitations include the limited availability of good *a priori* information about the solution and the lack of a "good" error metric. We describe an approach that combines body surface measurements and standard forward models with two additional information sources: statistical prior information about epicardial potential distributions and sparse simultaneous measurements of epicardial potentials made with multielectrode coronary venous catheters. We employ a Bayesian methodology which offers a general way to incorporate these information sources and additionally provides statistical performance analysis tools. In a simulation study, we first compare solutions using one or more of these information sources. Then, we study the effects of varying the number of sparse epicardial potential measurements on reconstruction accuracy. To evaluate accuracy, we used the Bayesian error covariance as well as traditional error metrics such as relative error. Our results show that including even sparsely sampled information from coronary venous catheters can substantially improve the reconstruction of epicardial potential distributions and that a Bayesian framework provides a feasible approach to using this information. Moreover, computing the Bayesian error standard deviations offers a means to indicate confidence in the results even in the absence of validation data.**

***Index Terms*—Bayesian estimation, forward/inverse modeling, inverse electrocardiography, inverse problems.**

I. Introduction

In INVERSE electrocardiography (ECG), one seeks to reconstruct cardiac electrical source distributions from body surface potentials [1], [2]. Despite many years of progress, successful clinical applications have been very rare. One basic limitation of these inverse solutions is the relatively low level of information about the cardiac sources present in the body surface potentials, due to attenuation and smoothing in the thorax. If we could acquire and make effective use of additional information sources, either general to an entire class of inverse problems or specific to the individual subject, it might help to achieve more accurate and more reliable inverse reconstructions than are otherwise possible. Clinicians make qualitative use of this strategy by combining body-surface ECGs with catheter-based electrical measurements to improve localization of ectopic activation or reentrant arrhythmias [3], [4]. The use of this information in a quantitative inverse solution is, however, an unexplored approach that we have addressed in this paper.

In this paper, we describe and evaluate an approach to epicardial potential-based inverse electrocardiography that combines body surface measurements and standard forward models with two additional information sources: statistical prior information about epicardial potential distributions estimated from a database of previous recordings and measurements of a small subset of the epicardial potentials made simultaneously with the torso-surface potential measurements through multielectrode coronary venous catheters.

To include this additional information, we have adopted a Bayesian framework because of the flexibility it provides in incorporating the three types of information sources we wished to study. The Bayesian framework achieves stable solutions via a statistical model for the unknown potentials, in contrast to the most common approach to solve for inversely computed epicardial potentials, which uses a deterministic model for the unknown potentials [5], [2]. Using deterministic models requires some form of regularization, most commonly in the Tikhonov framework [6], [7], to stabilize the solution against the very large and oscillatory reconstructed potentials caused by the ill-posed nature of the problem. In the simplest cases, Bayesian and Tikhonov solutions turn out to be equivalent, but in more complex scenarios they lead to distinct algorithms.

One additional advantage of the Bayesian formulation is the availability of *performance analysis* tools to statistically characterize solutions. The most common of these tools is the Bayesian error covariance, which gives a quantitative measure of the statistical reliability of a solution. It depends only on the mathematical formulation of the problem (here, the forward model, measurement geometry, etc.) and the probability model assumed for the sources and noise. It is not an *a posteriori* error metric such as relative error, which depends on specific measurements and on knowledge of the actual solution; rather, it is a statistical average or "prediction" quantity. In a companion study [8], we

Manuscript received September 15, 2005. This work was supported in part by the Center for Integrative Biomedical Computing NIH NCRR under Project 2-P41-RR12553-07. The work of Y. Serinagaoglu was supported by the Higher Education Council. *Asterisk indicates corresponding author.*

*Y. Serinagaoglu is with the Electrical and Electronics Engineering Department, Middle East Technical University, Ankara 06530, Turkey (e-mail: yserin@metu.edu.tr).

D. H. Brooks is with Northeastern University, Boston, MA 02115 USA.

R. S. MacLeod is with the University of Utah, Salt Lake City, UT 84102 USA.

Digital Object Identifier 10.1109/TBME.2006.881776

studied the feasibility of using the theoretical error covariance values in place of the actual error covariance values calculated from the error between the original potentials and the solutions. In this paper, we present examples to illustrate that the Bayesian error covariance can be used effectively to predict the performance we actually achieve using combinations of information sources, and that it may correspond more accurately to visual examination of reconstruction accuracy than does, for example, average relative error.

We have followed the lead of previous researchers [9]–[11] by adopting a Gaussian model for the unknown epicardial potential distributions as well as for the measurement noise and assuming that the potentials and the noise are mutually uncorrelated. In the Gaussian model, the prior probability density function and the measurement conditional probability densities can each be specified with a mean vector and a covariance matrix. Early investigation of Bayesian inverse electrocardiography by Martin *et al.* [9] showed the feasibility of applying statistical constraints to the epicardial potential distribution over a sphere with a radius of 4 cm surrounding the heart. The epicardial potentials were simulated from an activation sequence, and the mean vector and the covariance matrix were estimated from these simulated epicardial potentials using temporal averaging and Monte Carlo sampling. Barr *et al.* used a simplified probability model, assuming that the epicardial potentials were zero mean, mutually independent, and identically distributed (i.i.d.), resulting in a diagonal covariance matrix with entries equal to the epicardial potential power [10]. The measurement noise was also assumed to be i.i.d. and appropriate variance values were used for the epicardial potentials and measurement noise. This Bayesian formulation is equivalent to zero-order Tikhonov regularization, with the regularization parameter [λ^2 in (6) and (7)] equal to the ratio of the variance of the torso measurement noise to the variance of the (unknown) epicardial potentials.

More recent simulation studies conducted by van Oosterom [12], [13] showed that when there is good *a priori* information available about the epicardial potentials, in the form of a reasonably accurate full spatial covariance matrix, Bayesian estimation recovers considerable detail in the epicardial potential maps. Like Martin *et al.*, van Oosterom obtained the covariance matrix from simulated epicardial potentials. A related statistical approach proposed by Greensite [11], [14] combined temporal and spatial constraints to estimate temporal and spatial covariances under certain specific assumptions about structures inherent in the problem formulation. All of these methods concluded that using appropriate prior models, one can improve accuracy and reliability of inverse solutions, thus providing the motivation for our studies. None of these studies, however, have made use of the additional information that venous catheters can provide in order to formulate an inverse solution approach.

The use of error metrics based on statistical assumptions has a recent history in the inverse bioelectric field literature. Reports in inverse electroencephalography (EEG) and magnetoencephalography (MEG) describe approaches that employ statistical estimation methods to perform error analysis using Cramer–Rao bounds [15]–[17] and Bayesian methods [18]. In the latter study, Russell *et al.* employed a Bayesian estimation framework in a simple scenario with uncorrelated sources and found Bayesian performance analysis tools to be useful. These results motivated the use of the Bayesian estimation error covariance in this study for the inverse electrocardiography problem, in which the statistical model is more complicated due to spatial correlation of the sources. For simplicity, we ignored temporal correlation of the sources in this paper.

Of the two types of additional information we studied, incorporating previously recorded data to estimate prior statistics posed no new technical data acquisition problems. However, the use of epicardial venous catheters is still emerging and evolving. Recent advances in catheter technology allow the use of multiple venous catheters, each containing up to 16 electrodes, to map regions of the epicardial surface of the heart [19]–[21]. Previous studies showed that signals from such catheters were very similar to those recorded from nearby sites on the heart surface [22], thus allowing the simulation of catheter recordings with epicardial electrode recordings. These simulated venous catheter measurements have been used in previous studies together with a statistical prior estimated from previous epicardial recordings, in an *ad hoc* fashion, to estimate high resolution activation and/or potential maps of the complete epicardium [22]–[25].

In this paper, we formalized and broadened the statistical framework to include both estimation from limited epicardial lead sets and a combination of inverse solution and statistical estimation approaches. We compared the performance of the different combinations under experimental conditions and evaluated a statistical metric of uncertainty that offers quantitative estimates of the quality of the inverse solutions without knowledge of the actual solution. We also evaluated the effects of varying the number of epicardial leads included in the inverse solution and found that even small numbers of these signals substantially improved the accuracy of the solution.

II. Problem Definition

A. Torso Potentials and Forward Model

The forward model relates torso potentials to epicardial potentials and contains implicit information about the geometry of the epicardium and the body surface as well as the conductivity of the intervening volume conductor. The forward solution is a matrix $\mathbf{A}$, that linearly relates the epicardial potentials to the torso potentials according to

$$\mathbf{y}(i) = \mathbf{A}\,\mathbf{x}(i) + \mathbf{n}(i), i = 1, 2, \ldots, N_t \tag{1}$$

where $\mathbf{y}(i)$ is an $M \times 1$ vector of torso potentials at time instant i, $\mathbf{x}(i)$ is the associated $N \times 1$ vector of epicardial potentials, $\mathbf{A}$ is the $M \times N$ matrix representing the forward solution, $\mathbf{n}(i)$ is measurement noise of the same dimension as $\mathbf{y}(i)$, and i and N_t are the discrete time index and the number of time samples, respectively.

In this paper, we ignore the temporal correlation of the epicardial potentials. It has been well established [2], [11], [14] that this is suboptimal. However, we choose here to concentrate on the use of the spatial covariance without the complications

that would be introduced if spatio-temporal covariance were included.

B. Sparse Epicardial Potentials

We denote the sparse epicardial potentials (SEP) measurements available via unipolar electrodes (leads) on venous coronary catheters at N_k ($N_k < N$) locations as $\tilde{\mathbf{x}}_\mathbf{m}$. For convenience, we organize $\mathbf{A}$ and $\mathbf{x}$ such that the first N_k elements of $\mathbf{x}$ correspond to measured leads, and the first N_k columns of $\mathbf{A}$ are the coefficients that multiply these measured values of $\mathbf{x}$, i.e., $\mathbf{x} = [\mathbf{x_m}^T\ \mathbf{x_u}^T]^T$ and $\mathbf{A} = [\mathbf{A_m}\ \mathbf{A_u}]$ (where subscripts m and u represent "measured" and "unmeasured" leads, respectively, and superscript T denotes matrix transpose). To take into account noise in these epicardial measurements, we write

$$\tilde{\mathbf{x}}_\mathbf{m} = \mathbf{x_m} + \mathbf{e_m} \tag{2}$$

where $\mathbf{e_m}$ is the appropriately sized vector of noise components in the SEP measurements.

C. Augmented Formulation

To include such sparse epicardial potentials into the inverse problem formulation, we replace the problem defined by (1) with a formulation that combines (1) and (2)

$$\mathbf{v} = \mathbf{D}\,\mathbf{x} + \tilde{\mathbf{n}} \tag{3}$$

where

$$\mathbf{v} = \begin{bmatrix} \mathbf{y} \\ \tilde{\mathbf{x}}_\mathbf{m} \end{bmatrix},\ \tilde{\mathbf{n}} = \begin{bmatrix} \mathbf{n} \\ \mathbf{e_m} \end{bmatrix},\ \text{and}\ \mathbf{D} = \begin{bmatrix} \mathbf{A_m} & \mathbf{A_u} \\ \mathbf{I}_{k\times k} & \mathbf{0} \end{bmatrix} \tag{4}$$

and solve this augmented inverse problem for $\mathbf{x}$.

D. Basic Statistical Assumptions

We make the following basic assumptions about the unknown epicardial potentials $\mathbf{x}$ and the two measurement noise vectors $\mathbf{n}$ and $\mathbf{e_m}$.

1) $\mathbf{x} \sim \mathrm{N}(\bar{\mathbf{x}},\ \mathbf{C}_x)$, where

$$\bar{\mathbf{x}} = \begin{bmatrix} \bar{\mathbf{x}}_\mathbf{m} \\ \bar{\mathbf{x}}_\mathbf{u} \end{bmatrix}\ \text{and}\ \mathbf{C}_x = \begin{bmatrix} \mathbf{C}_{mm} & \mathbf{C}_{mu} \\ \mathbf{C}_{um} & \mathbf{C}_{uu} \end{bmatrix}.$$

2) $\mathbf{n} \sim \mathrm{N}(\mathbf{0},\ \mathbf{C}_n)$. We further assume that $\mathbf{n}$ is i.i.d. (i.e., $\mathbf{C}_n = \sigma_n^2\,\mathbf{I}$) and uncorrelated with $\mathbf{x}$.
3) $\mathbf{e_m} \sim \mathrm{N}(\mathbf{0},\ \mathbf{C}_e)$. $\mathbf{e_m}$ is also i.i.d. (with $\mathbf{C}_e = \sigma_e^2\,\mathbf{I}$) and uncorrelated with both $\mathbf{x}$ and $\mathbf{n}$.

E. Estimation of Prior Density

The statistical approaches we applied require an accurate prior probability density for the epicardial potential distribution, in this case defined as a mean vector $\bar{\mathbf{x}}$ and covariance matrix $\mathbf{C}_x$, even in the absence of specific knowledge of the solution. To create the prior, we assume availability of a training set of previously measured epicardial potentials from which we first extract the QRS intervals from each beat. Let $\mathbf{X_{qrs},}_\ell$ denote the $N \times T_\ell$ space–time matrix for the epicardial potentials from the QRS of beat ℓ, $\ell = 1, 2, \ldots, L$, where L is the total number of beats included in the training set. For consistency, we arrange the training data so that the first N_k rows of each $\mathbf{X_{qrs},}_\ell$ contain the signals from the catheter-measured leads. Then, the training dataset is defined as

$$\mathbf{X_{ds}} = [\,\mathbf{X_{qrs,1}}\quad \mathbf{X_{qrs,2}}\quad \ldots\quad \mathbf{X_{qrs,L}}\,] \tag{5}$$

where $\mathbf{X_{ds}}$ is of size $N \times T$ and $T = T_1 + T_2 + \cdots + T_L$. The sample mean and covariance can then be estimated from this training dataset by averaging over time.

In this formulation, we described the general approach used to estimate the parameters of the prior density. Specific details of the training set composition for the studies presented here can be found in Section IV.

III. Methods

A. Solution Approaches

In this section, we present deterministic and stochastic solution approaches that use one or more of the available information sources. Unlike the deterministic approaches such as Tikhonov regularization, in the Bayesian approach the epicardial potential distribution is assumed to be random. In the well-known Bayesian *maximum a posteriori* (MAP) estimation, the solution is chosen to maximize the posterior distribution of the sources given the measurements. The effect of this maximization is to choose the solution that is the most probable one in the sense of both being consistent with our prior probability model of how such solutions behave and the particular data and forward model for an individual measurement. With the statistical assumptions used here (i.e., for the Gaussian case), the MAP estimation is optimal both in the Bayesian sense (because it is the conditional mean of the sources given the measurements) and also in the sense of the minimum mean square error estimate (MMSE). For consistency with previous reports in this area [12], [13], we employ the designation MAP to describe these methods. A more detailed explanation of the Bayesian MAP approach can be found in [8].

We studied the following combinations of information sources (summarized in Table I).

1) Only torso potentials. The corresponding method is Tikhonov regularization (**TIKH**).
2) Torso and sparse epicardial potentials together. We call this approach *Tikhonov regularization using sparse epicardial potentials* (**TIKH-SEP**).
3) Torso potentials and a prior from the training set together in Bayesian MAP estimation (**MAP**).
4) All three available information sources together. Again, we used Bayesian estimation and called this approach *MAP using sparse epicardial potentials* (**MAP-SEP**).

TABLE I
SUMMARY OF APPROACHES TO INCLUDE AVAILABLE INFORMATION SOURCES WITH TORSO MEASUREMENTS (TOR), SPARSE EPICARDIAL MEASUREMENTS (SEP), AND PRIOR STATISTICS ESTIMATED FROM DATABASE (PRI). CELL WITH "+" SIGN MEANS THAT INFORMATION SOURCE OF THAT COLUMN IS USED IN METHOD OF THAT ROW

	TOR	SEP	PRI
TIKH	+		
TIKH-SEP	+	+	
MAP	+		+
MAP-SEP	+	+	+
EPI-EST		+	+

5) Only the sparse epicardial potentials and the prior from the database, without the torso potentials. The associated method, which we called *epicardial estimation* (**EPI-EST**), used a Bayesian framework, but without torso potentials it was not an inverse solution.

1) Torso Data Only: Tikhonov Regularization (TIKH): When we used only the torso measurements and a forward model, but no additional information sources, we solved (1) using zero-order Tikhonov regularization [5]

$$\hat{\mathbf{x}} = (\mathbf{A}^T\mathbf{A} + \lambda^2\mathbf{I})^{-1}\mathbf{A}^T\mathbf{y}. \tag{6}$$

Regularization parameters for this and the following Tikhonov solutions can be chosen by any of the many methods available in the literature [26]; in this paper, we have used the L-curve method.

2) Torso Data and Sparse Measurements Only: Tikhonov Regularization Using SEP (TIKH-SEP): When we simply added the information from the sparse epicardial measurements without the prior statistical model estimated from the database, we solved (3) using the same Tikhonov method, but applied to the augmented problem

$$\hat{\mathbf{x}} = (\mathbf{D}^T\mathbf{D} + \lambda^2\mathbf{I})^{-1}\mathbf{D}^T\mathbf{v}. \tag{7}$$

3) Torso Data and Training Set: Bayesian MAP Estimation: If we included the prior covariance model estimated from the database, but not the sparse epicardial measurements, we again solved (1), but this time using a Bayesian MAP approach. In a slightly more flexible formulation than that proposed by others [12], [13], we assumed the epicardial potentials to be Gaussian but did not require a zero mean and were able to write for the MAP solution [8]

$$\hat{\mathbf{x}} = (\mathbf{A}^T\mathbf{C}_n^{-1}\mathbf{A} + \mathbf{C}_x^{-1})^{-1}(\mathbf{A}^T\mathbf{C}_n^{-1}\mathbf{y} + \mathbf{C}_x^{-1}\bar{\mathbf{x}}). \tag{8}$$

The source of estimates for the mean and covariance came from the database of measured epicardial potentials.

4) All Three Information Sources: MAP Estimation Using SEP (MAP-SEP): When we included all three information sources, the resulting MAP estimation became

$$\hat{\mathbf{x}} = (\mathbf{D}^T\mathbf{C}_{\tilde{n}}^{-1}\mathbf{D} + \mathbf{C}_x^{-1})^{-1}(\mathbf{D}^T\mathbf{C}_{\tilde{n}}^{-1}\mathbf{v} + \mathbf{C}_x^{-1}\bar{\mathbf{x}}) \tag{9}$$

where $\mathbf{C}_{\tilde{n}}$ is the covariance matrix of the augmented noise vector $\tilde{\mathbf{n}}$

$$\mathbf{C}_{\tilde{n}} = \begin{bmatrix} \mathbf{C}_n & \mathbf{0} \\ \mathbf{0} & \mathbf{C}_e \end{bmatrix}.$$

5) No Torso Data: Epicardial Estimation (EPI-EST): For completeness, we considered the case in which we used sparse epicardial measurements and a prior from a database, but no torso measurements (and no forward model). This method is an adaptation of the activation time estimation algorithm in [22] to estimate epicardial potentials. Such an approach does not involve an inverse solution, but from the viewpoint of understanding the role of information sources it provided a relevant comparison with the true inverse solutions. The probability model follows Section II-D, but here we estimated only the unmeasured leads, given the sparse epicardial measurements and a prior model. To be consistent with the partitioning of $\mathbf{x}$ into $\mathbf{x_m}$ and $\mathbf{x_u}$, we partitioned the solution vector $\hat{\mathbf{x}}$ also into two parts: $[\hat{\mathbf{x}}_\mathbf{m}^T\ \hat{\mathbf{x}}_\mathbf{u}^T]^T$. Then, we set $\hat{\mathbf{x}}_\mathbf{m}$ exactly equal to $\tilde{\mathbf{x}}_\mathbf{m}$ and calculated $\hat{\mathbf{x}}_\mathbf{u}$ using the Bayesian MMSE estimate, which is equal to the posterior mean $E\{\mathbf{x_u}\backslash\tilde{\mathbf{x}}_\mathbf{m}\}$

$$\hat{\mathbf{x}}_\mathbf{u} = \bar{\mathbf{x}}_\mathbf{u} + \mathbf{C}_{um}\,\mathbf{C}_{\tilde{m}\tilde{m}}^{-1}\,(\tilde{\mathbf{x}}_\mathbf{m} - \bar{\mathbf{x}}_\mathbf{m}) \tag{10}$$

where $\mathbf{C}_{\tilde{m}\tilde{m}} = \mathbf{C}_{mm} + \mathbf{C}_e$ is the covariance matrix of $\tilde{\mathbf{x}}_\mathbf{m}$.

We stated earlier that under the statistical assumptions of this paper, the MMSE is also the MAP estimate. Thus, similarly to the previous two Bayesian approaches, the *epicardial estimation* method is also a MAP solution that uses the same prior density but a different measurement model.

B. Error Measures

A major difficulty in deciding which solution approach (i.e., which information source combination) provides the best results is to determine the most appropriate error metric with which to evaluate success. In this paper, we use the Bayesian error covariance matrix as the main evaluation tool for the Bayesian methods. We also include traditional error metrics, relative error and qualitative comparison of potential distributions, to evaluate the quality of the results.

1) Bayesian Error Maps: The Bayesian MAP reconstruction $\hat{\mathbf{x}}$ is unbiased under the Gaussian assumptions [27]. Therefore, the estimation error has zero mean and its covariance matrix is

$$\mathbf{C}_\epsilon = (\mathbf{A}^T\mathbf{C}_n^{-1}\mathbf{A} + \mathbf{C}_x^{-1})^{-1}. \tag{11}$$

Each diagonal element of this error covariance matrix gives the variance of the error in the estimate of the epicardial potential of the corresponding lead, i.e.,

$$\mathrm{var}(x_j - \hat{x}_j) = \mathbf{C}_\epsilon(j,j) \tag{12}$$

where x_j and $\hat{x}_j$ are the jth elements of $\mathbf{x}$ and $\hat{\mathbf{x}}$, respectively, and $\mathbf{C}_\epsilon(j,j)$ is the jth diagonal element of $\mathbf{C}_\epsilon$. Using this variance and the Bayesian MAP solution, one can calculate confi-

dence intervals for the estimate [8]. For example, with ≈95% probability the true solution $\hat{x}_j$ at lead j lies within the range

$$\hat{\mathbf{x}}_j - 2\sqrt{\mathbf{C}_\epsilon(j,j)} \leq \mathbf{x}_j \leq \hat{\mathbf{x}}_j + 2\sqrt{\mathbf{C}_\epsilon(j,j)}. \quad (13)$$

In order to observe these confidence intervals over the surface of the heart, we generated error standard deviation prediction maps by taking the square root of the diagonal entries of the error covariance matrix of (11) and mapping these values to their corresponding lead locations on the heart surface. The larger the error standard deviation values in a region, the wider the confidence intervals, meaning that we can expect less reliable estimation in that region.

2) Traditional Methods of Error Assessment: We used three additional methods to assess the error between reconstructed and original maps. The first was qualitative analysis of the epicardial maps using the visualization program *map3d* [28] to show shading and isopotential contours. The second and the third were calculations of relative error and correlation coefficient

$$\mathrm{RE}(i) = \frac{||\mathbf{x}(i) - \hat{\mathbf{x}}(i)||_2}{||\mathbf{x}(i)||_2}, i = 1, 2, \ldots, N_t \quad (14)$$

$$\mathrm{CC}(i) = \frac{\sum_k (\mathbf{x}_k(i) - \bar{\mathbf{x}}_k(i))(\hat{\mathbf{x}}_k(i) - \bar{\hat{\mathbf{x}}}_k(i))}{\sqrt{\sum_k (\mathbf{x}_k(i) - \bar{\mathbf{x}}_k(i))^2 \sum_k (\hat{\mathbf{x}}_k(i) - \bar{\hat{\mathbf{x}}}_k(i))^2}} \quad (15)$$

where i is the time index and k is the lead number. RE and CC are, respectively, the average relative error and the average correlation coefficient over the entire heart beat.

C. Simulation Experiments

To test our solution approaches for epicardial potential estimation under realistic conditions, we simulated torso surface and sparse epicardial potentials with canine epicardial measurements from two types of experiments performed at the Nora Eccles Harrison Cardiovascular Research and Training Institute at the University of Utah. In *in situ* experiments, the heart remained in the animal, exposed through a mid-sternal opening and suspended in a pericardial cradle. In *isolated heart* experiments, a preparation described previously [29] was used, consisting of an isolated dog heart suspended in a torso-shaped instrumented electrolytic tank. Our data came from experiments in which the heart was paced from the left or right ventricular epicardium. In both preparations, epicardial potentials were recorded simultaneously at 1000 samples/s from 490 epicardial sock electrodes sewn into a flexible nylon stocking fitted over the ventricles. Signal preprocessing consisted of gain correction of all channels, windowing of single beats of interest, then linear baseline adjustment of each signal using customized software.

We computed all the forward solutions for these studies from a homogenous torso geometry that included the epicardial sock electrodes (490 nodes and 976 triangles) and the torso tank (771 nodes and 1254 triangles). The forward solution used a boundary element formulation based on the method of Barr *et al.* [30] modified to use linear elements [31]. To mimic realistic measured potentials, we added independent, zero mean, Gaussian distributed noise at 25-dB signal-to-noise ratio (SNR) to the computed forward solutions. We chose this SNR value since it was approximately what we observed in true body surface recordings. To simulate the catheter measurements ($\hat{\mathbf{x}}_\mathbf{m}$), we first selected the sock leads that lay over the four major coronary veins [22], then added independent, zero mean, Gaussian-distributed noise to these selected leads at 30-dB SNR. Again, this SNR value was approximately what we observed in the true catheter recordings.

We simulated catheter measurements for three different lead numbers, $N_k = 14$, $N_k = 21$, and $N_k = 42$. Coverage achieved by the measurement locations was the same for all cases, but the sparsity of these locations varied with the number of measured leads.

IV. Results

We present two sets of results. The first is a comparison of all the solution methods described in Section III-A, while the second includes only the two methods that employ the Bayesian MAP approach (i.e., **MAP** and **MAP-SEP**), with variable numbers of sparse epicardial measurements. For both sets of results, we first present the Bayesian error standard deviation prediction of reconstruction variability (that is, the error covariance maps), then present the actual inverse-computed solutions. The error covariance maps, of course, can only be calculated for the Bayesian methods, so the Tikhonov solutions and the Bayesian solutions are compared with each other only using the traditional error metrics.

We ran our algorithms on various test beats from experiments with different animals, using different pacing locations, etc., using various training sets. In this paper, we show one typical example of these results; the data used for testing came from a left ventricularly (LV) paced test beat from an isolated heart experiment as described previously. The training set used for estimating prior statistics for the Bayesian methods included ten LV-paced beats (paced from five different sites located at the anterosuperior, posterolateral, and inferior LV regions) from two different experiments, one *in situ* and one in an isolated heart. The test beat came from an experiment (i.e., experimental animal) that was not included in the training set.

A. Comparison of All Solution Approaches

For this comparison of epicardial potential reconstructions, we set the number of sparse epicardial leads $N_k = 42$ (less than 10% of the number of nodes to be reconstructed), aligned along the major coronary veins. Regularization parameters for all Tikhonov approaches were determined using the L-curve method [7].

1) Error Maps: Fig. 1 shows the error standard deviation prediction maps corresponding to the three Bayesian approaches, **EPI-EST**, **MAP**, and **MAP-SEP**, presented as two different views of the same heart model. In these maps, light regions correspond to smaller standard deviations and dark regions to larger standard deviations. The color map range is the same for each map in Fig. 1 and the "isostandard deviation" contours were evenly spaced between 0 and 5 mV (maximum error standard deviation values corresponding to **MAP** and **MAP-SEP** are 5.33

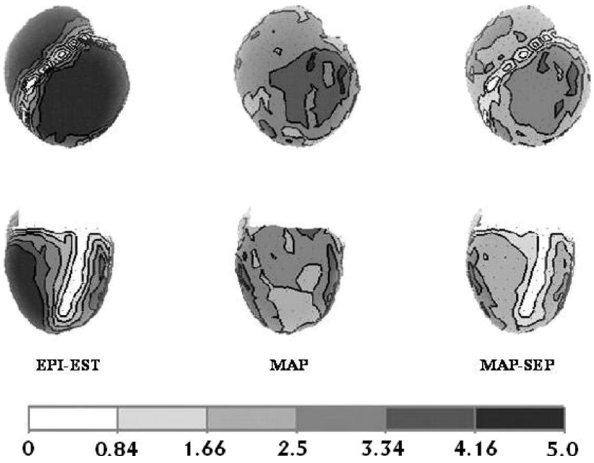

Fig. 1. Error standard deviation maps corresponding to three Bayesian methods, MAP, MAP-SEP, and EPI-EST. Top and bottom panels show different views of heart.

and 4.09 mV, respectively). The true maxima of error standard deviation values corresponding to **EPI-EST** were higher than shown here (approximately equal to 10 mV); for better visibility of **MAP** and **MAP-SEP** error maps, we clipped the scale on the **EPI-EST** maps.

We observed the following from the results.

1) The methods that used sparse epicardial measurements, i.e., **EPI-EST** and **MAP-SEP**, had much smaller predicted error standard deviation values around the measurement sites than in regions away from these sites.
2) **EPI-EST** produced very large error standard deviation values (much larger than those of **MAP** or **MAP-SEP**) away from the measurement sites.
3) The error standard deviations for the **MAP-SEP** reconstruction were, in general, smaller than those of the **MAP** reconstruction, even in the regions where there were no epicardial measurement leads.

2) Epicardial Potential Reconstructions: Isopotential maps of the original epicardial potentials and various solutions at three time instants are shown in Fig. 2. The figure has three panels from top to bottom, each corresponding to a different time sample, as noted, relative to the time of stimulus delivery. Each panel contains six maps; the upper left map shows the original epicardial distribution, while the other five show reconstructions by the five methods being compared. To the right of each panel is an electrogram selected from the original data with a vertical line illustrating the timing of that set of maps. In each panel, the range is fixed for all isopotential maps and we set the parameters of *map3d* to draw isopotential contours that were evenly spaced between the maximum and minimum of the original map. In these maps, darker regions represent negative potentials, lighter regions represent positive potentials, and the wavefront lies at the transition from darker to lighter regions. In the isopotential maps corresponding to each solution method, the relative error and correlation coefficient values at that time instant are given at the lower right corner of the map.

a) Comparison of Bayesian Approaches: In general, the **MAP-SEP** reconstructions achieved better fidelity to the original isopotential maps than the **MAP** reconstructions. In the

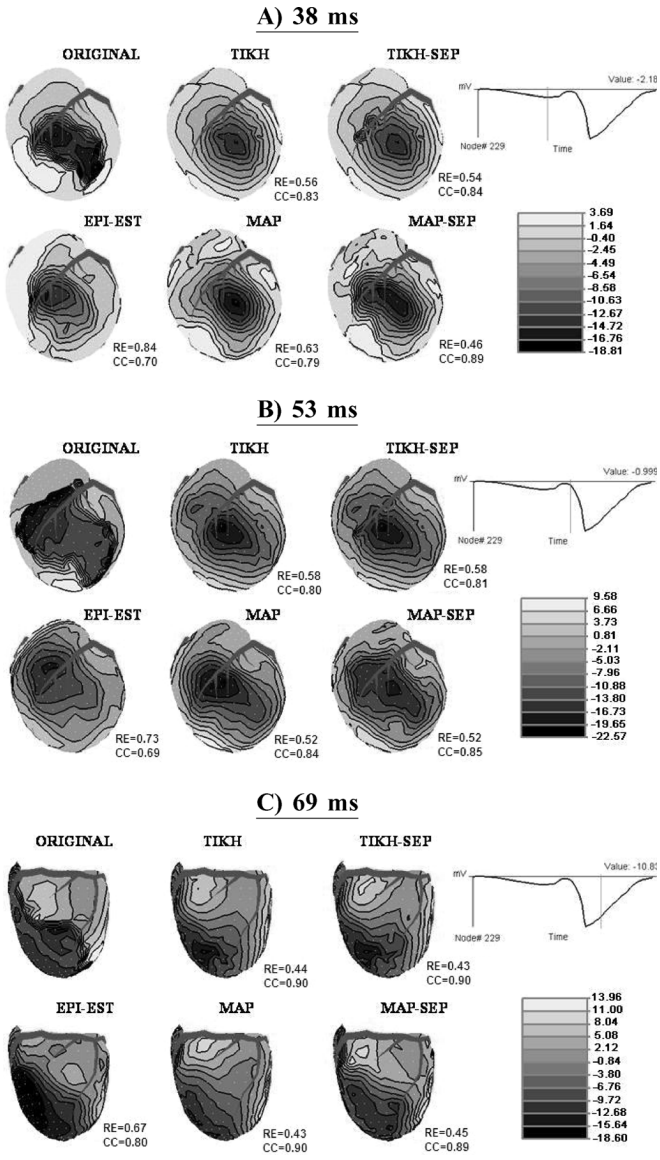

Fig. 2. All solution methods are compared. Original and estimated epicardial potentials for a left ventricularly paced beat using LV-paced training set. Panels A, B, and C show potentials at 38, 53, and 69 ms after stimulus, respectively. Dark regions correspond to more negative potentials and light regions to more positive potentials. Relative error for each method at corresponding time instant is given at lower right corner of each map. Schematic drawing of coronary arteries was included for reference.

EPI-EST approach, the reconstruction was almost as good as **MAP-SEP** near the measurement sites, but of poor quality elsewhere. Specifically, at 38 ms, **MAP** reconstructed a wavefront propagation pattern that looked more circular than the elliptical shape of the original, while **MAP-SEP** reconstructed an elliptical wavefront. Moreover, **MAP-SEP** captured the narrowness of the wavefront better than **MAP**, as indicated by the closer spacing of the isopotential lines. **EPI-EST** reconstructed the tight wavefront with good fidelity to the original around the 8 o'clock position, near the measurement sites, better than **MAP** and comparable to **MAP-SEP**. However, away from the measurement sites, the wavefront became even more spread out and smoothed than for **MAP**. At 53 ms, the original wavefront propagated almost parallel to the left anterior descending (LAD)

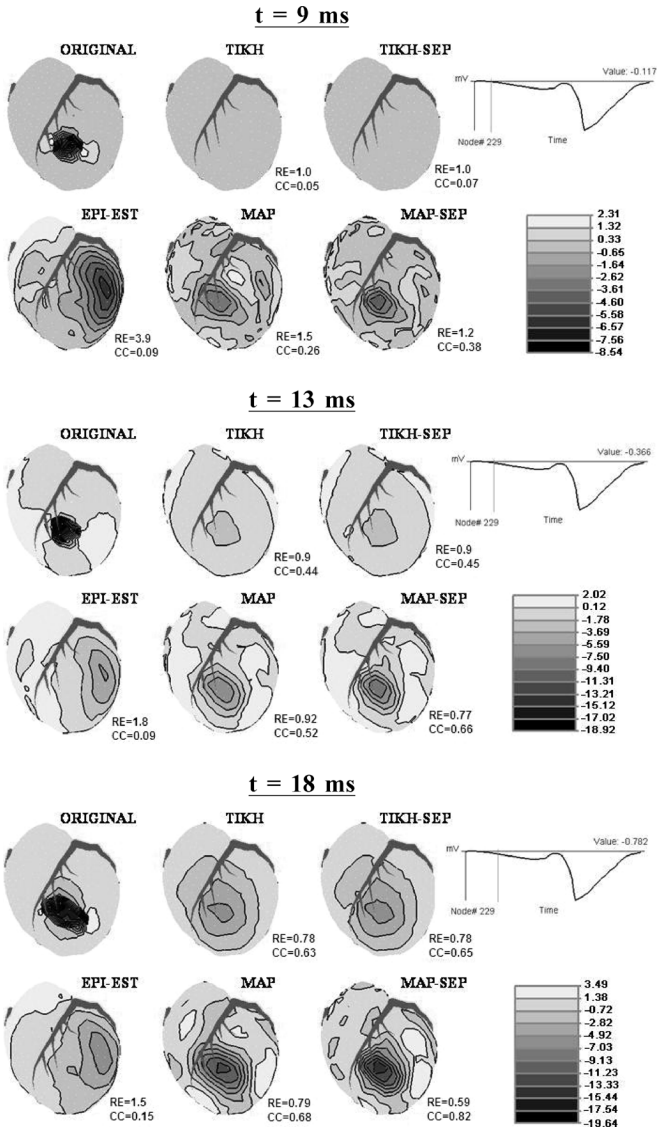

Fig. 3. Earliest observation of wavefront near stimulus site. Original and estimated epicardial potentials for same test beat and training set as in Fig. 2 but at different time instants. Panels A, B, and C show potentials at 9, 13, and 18 ms after stimulus, respectively. Arrangement of figure is similar to previous figure of potential maps. (A) $t = 9$ ms. (B) $t = 13$ ms. (C) $t = 18$ ms.

artery on the right ventricle. The wavefront reconstructed by **MAP** was spread out in a round shape into the RV and did not reproduce this parallel wave propagation shape. **MAP-SEP** reconstructed the more linear shape of the original. At this time instant, the original wavefront had moved away from the measurement sites, and **EPI-EST** did not reliably localize the wavefront; it produced a general fit to the original wavefront, but the reconstruction was very spread out and smoothed. Finally, at 69 ms, the wavefront that lay along the 10 o'clock – 4 o'clock line was spread out in the **MAP** reconstruction, while the wavefront reconstructed by **MAP-SEP** was more similar to the original. The wavefront reconstructed by **EPI-EST** had better fidelity to the original than **MAP**; it was close to the performance of **MAP-SEP**. But although the wavefront structure was well captured in both **EPI-EST** and **MAP-SEP**, the **EPI-EST** orientation was shifted slightly compared to the original and the wavefront again started to spread out around the 6 o'clock position. Moreover, **EPI-EST** distorted the amplitude of the negative region that lies to the left of the wavefront around the 8 o'clock position; it was much more negative (darker in color) than the original and the other solutions.

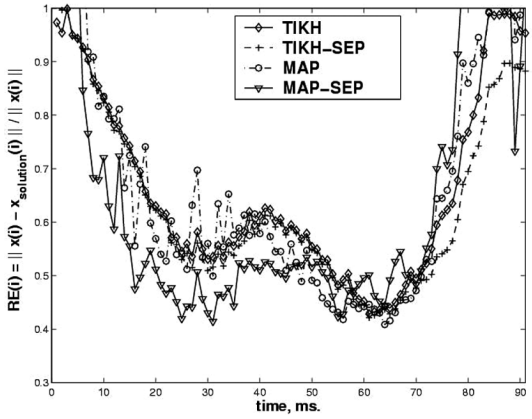

Fig. 4. RE of each inverse solution across all frames in QRS region. Note that at beginning and end of QRS region, RE values are sometimes larger than one, but we clipped graph at upper limit of one.

b) Tikhonov Regularization Versus Bayesian Methods: In general, Tikhonov regularization with or without sparse epicardial potentials produced spatially smooth results with poor reproduction of the waveshape. **MAP** and **MAP-SEP** recovered the potentials more successfully than did Tikhonov regularization. **EPI-EST** reconstructions were also better than the Tikhonov regularized reconstructions near the measurement sites but were either comparable or worse at other locations.

c) Detection of Stimulus Site: One error metric of interest in the context of clinical application of an electrocardiographic inverse problem is the ability to locate the site of earliest activation on the epicardium. Fig. 3 shows three time instants close to stimulus application time ($t = 0$ ms) and illustrates the superiority of the two Bayesian inverse solutions over the Tikhonov solutions. In the reconstructions with **MAP** and **MAP-SEP**, the stimulus site first appeared at 9 ms, whereas with Tikhonov methods, the first appearance was delayed until 13 ms. Even then, the wavefront was still too spread to properly localize the stimulus site. Similarly, **EPI-EST** did not localize the stimulus site properly even at 18 ms.

d) Relative Errors (RE) and Correlation Coefficients (CC): Statistical metrics, such as RE and CC, provided somewhat equivocal results that require careful analysis. As shown in Fig. 4, during most of the QRS region, **MAP-SEP** produced slightly smaller RE values than the two Tikhonov methods and **MAP**, but in the second half of the QRS, the pattern reversed. This finding suggests that it was during the rapidly changing portion of the spread of activation that the advantages of Bayesian approaches were most apparent. In contrast, during the smoother changing portion, the Tikhonov methods performed better in terms of RE so that the average RE values, shown in Table II, were slightly superior for the Tikhonov approaches compared to the Bayesian. CC values, whose averages for each method are also shown in Table II, also did not reflect the significant observations that we made on the epicardial reconstructions.

TABLE II
AVERAGE OF RE AND CC OVER QRS INTERVAL AND THEIR STANDARD DEVIATIONS (STD), COMPARED FOR VARIOUS ESTIMATION METHODS

	average RE	std of RE	average CC	std of CC
TIKH	0.65	0.17	0.65	0.27
TIKH-SEP	0.63	0.16	0.69	0.25
MAP	0.71	0.38	0.69	0.26
MAP-SEP	0.69	0.39	0.71	0.25
EPI-EST	1.31	1.06	0.51	0.27

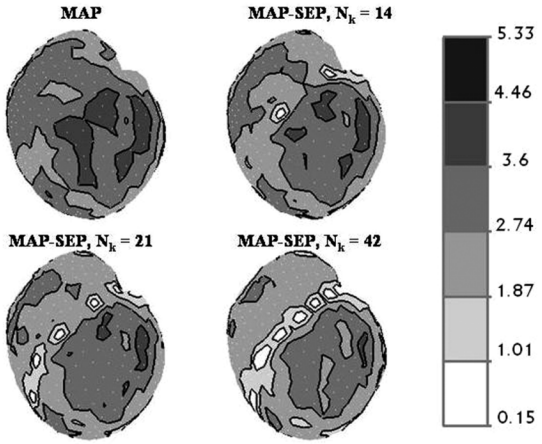

Fig. 5. Estimation error standard deviation precition maps corresponding to MAP and MAP-SEP with $N_k = 14, 21,$ and 42.

When interpreting such results, it is important to take into account previous studies [24] which have suggested that relative error and similar statistical metrics can hide features of the reconstructed potential maps that have physiologic importance. In this paper, we again observed such discrepancies when comparing the ability of the different approaches to identify the earliest site of activation, as described previously. Similarly, comparing the maps in Figs. 2 and 3 showed qualitative differences between the two classes of methods that were not visible from RE plots.

B. Effects of Number of Measured Epicardial Leads

1) Error Maps: Fig. 5 contains estimation error prediction maps when the number of measured epicardial leads are varied. In general, the error standard deviation predictions decrease with the addition of measured epicardial potentials. In order to quantify the error standard deviation (SD) improvements with the addition of sparse epicardial potentials, we calculated the percentage of leads on the heart surface whose error SDs fell within different 95% confidence intervals. From these percentages, we created the cumulative distribution functions shown in Fig. 6, in which the x axis shows the 95% confidence range (i.e., two times error standard deviation values, which corresponds to two times the boundary of each gray scale level in Fig. 5) and the y axis shows the percentage of leads on the heart surface. Different line styles correspond to the **MAP** method ($N_k = 0$) and the **MAP-SEP** method with varying N_k (14, 21, 42). When we used **MAP-SEP** with $N_k = 42$, about 90% of the leads had epicardial potential estimates that were within the 95% confidence range $\hat{\mathbf{x}}_j - 4.04 \leq \mathbf{x}_j \leq \hat{\mathbf{x}}_j + 4.04$

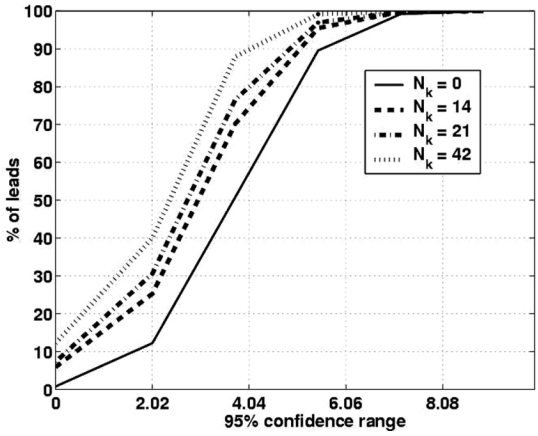

Fig. 6. Cumulative distribution function that shows percentage of leads that fall within each error standard deviation interval for MAP and MAP-SEP with $N_k = 14, 21,$ and 42. x axis shows 95% confidence ranges (i.e., two times error standard deviation values in millivolts), which correspond to two times the boundary of each gray scale level in Fig. 5, and y axis shows percentage of leads on heart surface. Each method is represented with different line style, as shown in legend.

[see (13)]. As N_k became smaller, the curve shifted to the right and the confidence range became wider, meaning there was less confidence in the estimate. There was a significant improvement in the confidence range by adding as few as $N_k = 14$ epicardial measurements compared to **MAP**. Increasing N_k from 14 to 21, on the other hand, did not improve the confidence range as much as increasing N_k from 21 to 42.

2) Epicardial Potential Reconstructions: In Fig. 7, we plot the isopotential maps of the heart surface of the original beat and various inverse solutions. We show the isopotential maps for the same three time instants as in Fig. 2. The RE and CC values at that time instant are now given at the lower left corner of the maps. The maps clearly indicate a consistent and progressive improvement in the reconstruction by adding the known leads. The improvement is visible at all three time instants through a better rendering of the wave front (region of high contour density).

V. DISCUSSION AND CONCLUSION

The main goal in this paper was to evaluate the potential advantages for inverse ECG obtained by combining standard body surface mapping measurements and standard forward models with other information sources. We treated two candidate additional information sources: statistical prior information on epicardial potential distributions estimated from a database of previous recordings, and high-quality measurements of a small subset of the epicardial potentials made simultaneously with the torso surface potential measurements through catheter-mounted electrodes. We adopted a Bayesian framework because of the flexibility it provides to incorporate this range of information sources. The Bayesian formulation has the additional advantage of providing performance analysis tools to statistically characterize the solution methodology. We used the Bayesian error covariance to obtain a quantitative measure of the statistical reliability of a solution. We tested our methods using a combination of canine epicardial recordings

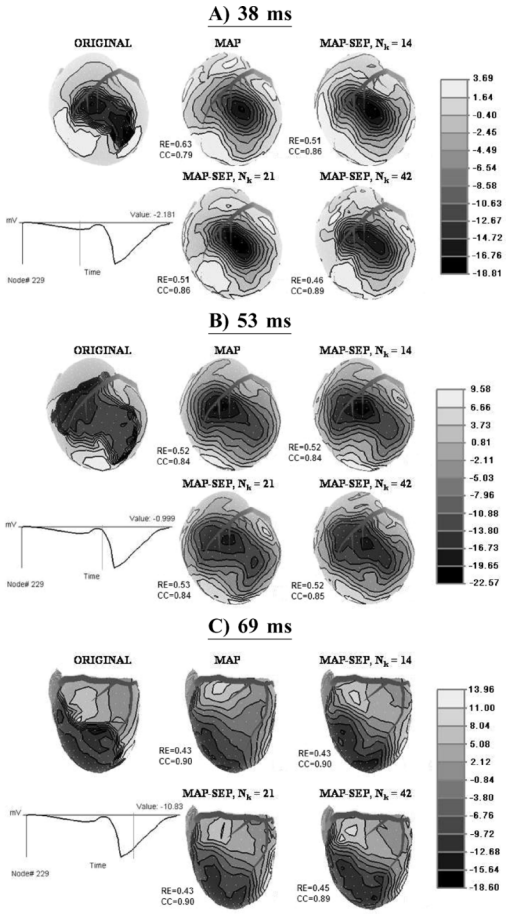

Fig. 7. Effects of number of measured epicardial leads. Original and estimated epicardial potentials for a left ventricularly paced beat using LV-paced training set. Panels A, B, and C show potentials at 38, 53, and 69 ms after stimulus, respectively. Arrangement of figure is similar to previous figure of potential maps except that electrogram has been moved to beneath the map of the original data and RE and CC values are now given at lower left corner of maps.

and simulated torso potentials. Our results showed that combining different information sources improved the quality of the inverse solutions. We also were able to show that Bayesian error covariance provides a powerful means of predicting the degree of confidence (and the associated error) without the need for prior knowledge of the solution.

Our main observation of the results was that using all three information sources yielded better wavefront reconstructions than using any one of the information sources alone or even any combination in pairs. Furthermore, this improvement was predicted by the error covariance maps. Specific observations that support this main point are as follows.

1) In the absence of prior information, using Tikhonov regularization, adding sparse epicardial potentials to torso measurements only improved the reconstructions slightly. This improvement was only near the measurement sites; away from the measurement sites, there was no difference between **TIKH** and **TIKH-SEP** reconstructions.
2) When we included prior information in the inverse solution and used Bayesian MAP estimation (**MAP** and **MAP-SEP**), we got better results than those obtained using Tikhonov regularization (with or without sparse epicardial measurements). This observation, combined with the previous one, confirms the findings in [12] and [13] that including prior information about the epicardial potentials improves the reconstructions, especially if we can obtain a reasonable set of epicardial data to create a training set.
3) When we only used sparse epicardial potentials and the prior information (i.e., when we applied **EPI-EST**), the fidelity of the reconstructed wavefront to the original was lost at locations even a short distance away from the measurement sites, while inverse solutions (even using Tikhonov regularization) reconstructed the wavefront more accurately than **EPI-EST**. This result demonstrated that we can gain valuable information by including the torso potentials and the forward model.
4) When we compared the error covariance maps corresponding to **MAP** and **MAP-SEP** reconstructions, we observed that the predicted error variances were usually smaller for **MAP-SEP** than for **MAP**. The corresponding inverse solutions agreed with this prediction: wavefront shape and extent was reconstructed more accurately with **MAP-SEP** than with **MAP**.
5) Bayesian-based inverse solution methods, i.e., **MAP** and **MAP-SEP**, were more successful at finding the stimulus site than the Tikhonov solutions and **EPI-EST**.

The second main observation from this paper was that in the error covariance maps, the standard deviation values became smaller over the heart surface when the number of epicardial measurement sites increased; around the measurement sites, error standard deviation values became very small (practically zero), meaning that confidence in the reliability of the reconstructions increased with the addition of sparse epicardial potentials. The corresponding inverse solutions also supported this finding, i.e., we obtained better reconstructions as the number of epicardial measurement sites increased. Detailed observations follow.

1) Comparing all four cumulative distribution functions we obtained from the error covariance maps, we observed that the 95% confidence range was achieved at a much smaller value when we used $N_k = 42$ than $N_k = 21$ or 14, whereas there was not a big difference between the confidence ranges of the latter two. On the other hand, the confidence range improved when we included only a small number of epicardial leads (i.e., $N_k = 14$) compared to solutions without them (i.e., **MAP**).
2) **MAP-SEP** and **EPI-EST** error standard deviation maps had significantly smaller error standard deviation values around the sparse epicardial measurement sites than those of the **MAP** approach.
3) A significant outcome of these observations is that one could design a sparse epicardial measurement scheme using the error covariance maps and the corresponding cumulative distribution functions. There are two main parameters in this design, the number of leads and their locations; for practical purposes, an optimal design will be a combination that additionally reflects the limitations of electrode design and placement. One possible tool for determining optimized designs is the predicted cumulative distribution function (cdf). For example, if there are

$i = 1, \ldots, P$ different N_{ki} values with varying spatial coverages available such that $N_{k1} < N_{k2} < \cdots < N_{kP}$, one could decide to use N_{ki} instead of $N_{k(i+1)}$ if the improvement in cdf percentages going from N_{ki} to $N_{k(i+1)}$ were not significant compared to the improvement going from $N_{k(i-1)}$ to N_{ki}. Alternatively, one could take advantage of the finding that around the measurement sites, error standard deviation decreases; if the error standard deviation maps show large values for a region, which means the reconstructions in that region will be less reliable, one could attempt to place sparse epicardial measurements nearby to reduce the error standard deviation and increase reliability of the reconstruction. If the region with the high error standard deviation were to lie near a major coronary vein, one could obtain epicardial potentials directly using intravenous catheters. If the region with high error standard deviation were away from the veins, one might employ electrodes inserted through the thorax to contact the heart surface [32]; such electrodes are not restricted to coronary vein locations.

There are, however, still some open questions and possible shortcomings of the methods we have proposed.

1) All evaluations of the methods presented here were carried out on ventricularly paced beats. Obviously, such beats present a much simpler and more organized propagation pattern, one that may indeed be more predictable with a correlation approach. Thus, all the results should be taken as directly applicable only to such beats; although, we believe that many of the conclusions will carry over to supra-ventricularly paced beats.
2) We used only the spatial correlations while neglecting the temporal correlations. However, epicardial potentials are clearly correlated in time and including these correlations in addition to the spatial ones would result in a more complete statistical model.
3) We used the Bayesian error covariance maps without attention to the error in the prior model. In a companion study [8], we showed that the similarity between the theoretical error covariance and actual error covariance calculated from the error between the original potentials and the solutions depends on how well the prior model represents the epicardial potentials. In order to establish the error covariance maps as a valid and robust evaluation tool, one should study the uncertainties in the error covariance maps due to errors in the prior covariance matrix estimation. One way to achieve this would be to evaluate the sensitivity of $\mathbf{C}_\epsilon$ in (11) to deviations in $\mathbf{C}_x$.
4) Previous studies have shown that the better the prior model, the better the reconstructions [24]. Here, we assumed that the training set was good and did not try to identify the best training set. However, even with this training set, we obtained results that encouraged us to pursue further application of Bayesian estimation and evaluation tools. In order to improve the results, one could develop automatic and robust methods to create a training set that best fit the data. One way to achieve this might be to estimate the epicardial potentials and the prior statistics simultaneously in an iterative fashion, e.g., using an expectation-maximization-type approach [33]. Another way would be to pick the training set that best fits the measurements, an approach we have already addressed in preliminary fashion [8].
5) We neglected geometric errors and errors in the noise model. These errors should be studied and, in fact, could be included in the statistical framework.

TABLE III
AVERAGE OF RE AND CC OVER QRS INTERVAL AND THEIR STANDARD DEVIATIONS (STD), COMPARED FOR BAYESIAN MAP ESTIMATION FOR VARYING NUMBER OF SPARSE EPICARDIAL MEASUREMENTS. VALUES FOR TIKHONOV REGULARIZATION, **TIKH**, ARE ALSO INCLUDED FOR COMPARISON

	average RE	std of RE	average CC	std of CC
TIKH	0.65	0.17	0.65	0.27
MAP	0.71	0.38	0.69	0.26
MAP-SEP, $N_k = 14$	0.67	0.33	0.71	0.25
MAP-SEP, $N_k = 21$	0.67	0.34	0.72	0.24
MAP-SEP, $N_k = 42$	0.69	0.39	0.72	0.24

The methods proposed in this paper are not specific to inverse electrocardiography problem in terms of epicardial potential distributions. On the contrary, other types of inverse problems could use these ideas to improve the accuracy and reliability in their respective research areas using the following approaches.

1) Incorporating various information sources in a Bayesian framework can be extended to other types of inverse problems. For example, endocardial mapping data via noncontact electrodes can be combined with sparse endocardial measurements via contact electrodes. Rao *et al.* presented an inverse solution in which both endocardial mapping data via noncontact electrodes and sparse endocardial measurements via contact electrodes were available, but the latter were used just for validation [34]. These measurements could be combined to improve the inverse solution.
2) Estimation error covariance can be used to evaluate other types of inverse problems. Russell *et al.* showed feasibility of this idea when both the sources and the measurement noise are i.i.d. This idea could easily be extended in a similar fashion to our derivation to handle full prior covariance matrices, such as the one used in the inverse EEG/MEG problem of [35].

ACKNOWLEDGMENT

The authors would like to thank Dr. B. Taccardi for his assistance in obtaining the experimental data and B. Yilmaz for his assistance in preparing data for analysis.

REFERENCES

[1] R. M. Gulrajani, "The forward and inverse problems of electrocardiography," *IEEE Eng. Med.*, vol. 17, pp. 84–101, Sep./Oct. 1998.
[2] R. S. MacLeod and D. H. Brooks, "Recent progress in inverse problems in electrocardiography," *IEEE Eng. Med.*, vol. 17, pp. 73–83, Jan. 1998.
[3] S. Pogwizd and P. Corr, "Reentrant and nonreentrant mechanisms contribute to arrhythmogenesis during early myocardial ischemia: Results using three-dimensional mapping," *Circ. Res.*, vol. 61, no. 3, pp. 352–371, 1987.
[4] A. SippensGroenewegen, H. Spekhorst, N. van Hemel, J. Kingma, R. Hauer, M. Janse, and A. Dunning, "Body surface mapping of ectopic left and right ventricular activation: QRS spectrum in patients without structural heart disease," *Circ.*, vol. 82, pp. 879–896, 1990.
[5] Y. Rudy and B. J. Messinger-Rapport, "The inverse problem in electrocardiography: Solutions in terms of epicardial potentials," *CRC Crit. Rev. Biomed. Eng.*, vol. 16, no. 3, pp. 215–268, 1988.

[6] A. N. Tikhonov and V. Y. Arsenin, *Solutions of Ill-Posed Problems*. New York: Halsted, 1977.
[7] P. C. Hansen, "Analysis of discrete ill-posed problems by means of the L-curve," *SIAM Rev.*, vol. 34, no. 4, pp. 561–580, 1992.
[8] Y. Serinagaoglu, D. H. Brooks, and R. S. MacLeod, "Bayesian solutions and performance analysis in bioelectric inverse problems," *IEEE Trans. Biomed. Eng.*, vol. 52, no. 8, pp. 1009–1020, Aug. 2005.
[9] R. O. Martin, T. C. Pilkington, and M. N. Morrow, "Statistically constrained inverse electrocardiography," *IEEE Trans. Biomed. Eng.*, vol. BME-22, pp. 487–492, Nov. 1975.
[10] R. C. Barr and M. S. Spach, "Inverse calculation of QRS-T epicardial potentials from body surface potential distributions for normal and ectopic beats in the intact dogs," *Circ. Res.*, vol. 42, pp. 661–675, 1978.
[11] F. Greensite, "A new treatment of the inverse problem of multivariate analysis," *Inverse Problems*, vol. 18, pp. 363–379, 2002.
[12] A. van Oosterom, "The use of spatial covariance in computing pericardial potentials," *IEEE Trans. Biomed. Eng.*, vol. 46, no. 7, pp. 778–787, Jul. 1999.
[13] ——, "The spatial covariance used in computing the pericardial potential distribution," in *Computational Inverse Problems in Electrocardiography*. P. R. Johnston, Ed. Southampton, U.K.: WIT, 2001, pp. 1–50.
[14] F. Greensite, "The temporal prior in bioelectromagnetic source imaging problems," *IEEE Trans. Biomed. Eng.*, vol. 50, no. 9, pp. 1152–1159, Sep. 2003.
[15] J. C. Mosher, M. E. Spencer, R. M. Leahy, and P. S. Lewis, "Error bounds for EEG and MEG dipole source localization," *Electroensephalography Clinical Neurophysiol.*, vol. 86, pp. 303–321, 1993.
[16] J. Malmivuo, V. Suihko, and H. Eskola, "Sensitivity distributions of EEG and MEG measurements," *IEEE Trans. Biomed. Eng.*, vol. 44, no. 2, pp. 196–208, Feb. 1997.
[17] C. H. Muravchik and A. Nehorai, "EEG/MEG error bounds for a static dipole source with a realistic head model," *IEEE Trans. Signal Process.*, vol. 49, no. 3, pp. 470–484, Mar. 2001.
[18] G. S. Russell, R. Srinivasan, and D. M. Tucker, "Bayesian estimates of error bounds for EEG source imaging," *IEEE Trans. Med. Imag.*, vol. 17, no. 6, pp. 1084–1089, Jun. 1998.
[19] A. D'Avila and P. Brugada, "Letter to the editor," *PACE*, vol. 17, pp. 1832–1833, 1994.
[20] C. Stellbrink, B. Diem, P. Schauterte, K. Ziegert, and P. Hanrath, "Transcoronary venous radiofrequency catheter ablation of ventricular tachycardia," *J. Cardiovasc. Electrophysiol.*, vol. 8, pp. 916–921, 1997.
[21] A. de Paola, W. Melo, M. Tavora, and E. Martinez, "Angiographic and electrophysiological substrates for ventricular tachycardia mapping through the coronary veins," *Heart (CEN)*, vol. 79, no. 1, pp. 59–63, 1998.
[22] R. O. Kuenzler, R. S. MacLeod, B. Taccardi, Q. Ni, and R. L. Lux, "Estimation of epicardial activation maps from intravascular recordings," *J. Electrocardiol.*, vol. 32, no. 2, pp. 77–92, 1999.
[23] R. S. MacLeod, B. Yilmaz, B. Taccardi, B. Punske, Y. Serinagaoglu, and D. H. Brooks, "Direct and inverse methods for cardiac mapping using multielectrode catheter measurements," *Biomedizinische Technik*, vol. 46 (supp), pp. 207–209, 2001.
[24] Y. Serinagaoglu, R. S. MacLeod, B. Yilmaz, and D. H. Brooks, "Multielectrode venous catheter mapping as a high quality constraint for electrocardiographic inverse solution," *J. Electrocardiol.*, vol. 35 (suppl), no. 4, pp. 65–73, 2002.
[25] B. Yılmaz, R. MacLeod, B. Punske, B. Taccardi, and D. Brooks, "Venous catheter based mapping of epicardial ectopic activation: Training set selection for statistical estimation," *IEEE Trans. Biomed. Eng.*, vol. 52, no. 11, pp. 1823–1831, Nov. 2005.
[26] P. C. Hansen, *Rank-Deficient and Discrete Ill-Posed Problems: Numerical Aspects of Linear Inversion*. Philadelphia, PA: SIAM, 1998, p. 247.
[27] S. M. Kay, *Fundamentals of Statistical Signal Processing: Estimation Theory*. Englewood Cliffs, NJ: Prentice-Hall, 1993, ch. 10–12.
[28] R. S. MacLeod and C. R. Johnson, "Map3d: Interactive scientific visualization for bioengineering data," in *Proc. Eng. Med. Biol. Soc. 15th Annu. Int. Conf.*, 1997, vol. 44, pp. 196–208.
[29] R. MacLeod, R. Lux, and B. Taccardi, "A possible mechanism for electrocardiographically silent changes in cardiac repolarization," *J. Electrocardiol.*, vol. 30, no. Suppl, pp. 114–121, 1997.
[30] R. Barr, M. Ramsey, and M. Spach, "Relating epicardial to body surface potential distributions by means of transfer coefficients based on geometry measurements," *IEEE Trans Biomed. Eng.*, vol. 24, pp. 1–11, Jan. 1977.
[31] R. MacLeod, R. Miller, M. Gardner, and B. Horáček, "Application of an electrocardiographic inverse solution to localize myocardial ischemia during percutaneous transluminal coronary angioplasty," *J. Cardiovasc. Electrophysiol.*, vol. 6, pp. 2–18, 1995.
[32] V. Y. Reddy *et al.*, "Combined epicardial and endocardial electroanatomic mapping in a porcine model of healed myocardial infarction," *Circulation*, vol. 107, pp. 3236–3242, 2003.
[33] A. P. Dempster, N. M. Laird, and D. B. Rubin, "Maximum likelihood from incomplete data via the EM algorithm," *J. Roy. Stat. Soc. Ser. B*, vol. 39, no. 1, pp. 1–38, 1977.
[34] L. Rao and D. S. Khoury, "System and methods for electrical-anatomical imaging of the heart," in *Proc. Second Joint EMBS-BMES Conf.*, 2002.
[35] J. W. Philips, R. M. Leahy, and J. C. Mosher, "MEG-based imaging of focal neuronal current sources," *IEEE Trans. Med. Imag.*, vol. 16, no. 6, pp. 338–348, Jun. 1997.

Yeşim Serinagaoglu (S'93–M'03) received the B.S. and M.S. degrees in electrical and electronics engineering from Middle East Technical University, Ankara, Turkey, in 1995 and 1997, respectively, and the Ph.D. degree from Northeastern University, Boston, MA, in 2003.

She is currently an Assistant Professor of Electrical and Electronics Engineering at Middle East Technical University. She is also a member of the Institute of Applied Mathematics at the same university. Her research interests include statistical and digital signal processing, with particular application to biomedical problems. Specific current interests include forward and inverse problems in electrocardiography, modeling the electrical activity of the heart and electrocardiography signal processing.

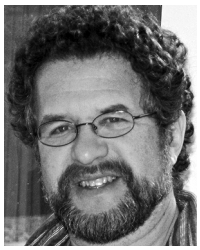

Dana H. Brooks (M'97–SM'06) received the B.A. degree in English from Temple University, Philadelphia, PA, in 1972, and the BSEE, MSEE, and Ph.D. degrees in electrical engineering from Northeastern University, Boston, MA, in 1986, 1988, and 1991, respectively.

He is an Associate Professor of electrical and computer engineering, the Associate Director of the Center for Communications and Digital Signal Processing, and PI of the BioMedical Imaging and Signal Processing Laboratory, at Northeastern, and a member of the Center for Integrative Biomedical Computing headquartered at the University of Utah. He was a Visiting Professor from 1999 to 2000 at the Universität Politecnica de Catalunya, Barcelona, Spain. His research interests include application of statistical and digital signal and image processing to biomedical signal processing and medical and biological imaging and open-source software systems for these applications.

Robert S. MacLeod (S'87–M'87) received the B.S. degree in engineering physics and the Ph.D. degree in physiology and biophysics from Dalhousie University, Halifax, Nova Scotia, Canada, in 1979 and 1990, respectively. He received the M.S. degree in electrical engineering from the Technische Universitat, Graz, Austria, in 1985.

He is an Associate Professor in the Bioengineering Department and the Department of Internal Medicine (Division of Cardiology) at the University of Utah, Salt Lake City, and an Associate Director of the Scientific Computing and Imaging Institute and the Nora Eccles Harrison Cardiovascular Research and Training Institute. His research interests include computational electrocardiography (forward and inverse problems), experimental investigation and clinical detection of cardiac ischemia and repolarization abnormalities, and scientific computing and visualization.